Chemical Geology 351 (2013) 299–309

Contents lists available at SciVerse ScienceDirect

Chemical Geology

journal homepage: www.elsevier.com/locate/chemgeo

# Comparison of the kinetic rate law parameters for the dissolution of natural and synthetic autunite in the presence of aqueous bicarbonate ions

Ravi K.P. Gudavalli [a,b], Yelena P. Katsenovich [a,*], Dawn M. Wellman [c], Melina Idarraga [a], Leonel E. Lagos [a], Berrin Tansel [b]

[a] Applied Research Center, Florida International University, 10555 W Flagler St., Suite 2100, Miami, FL 33174, USA
[b] Department of Civil and Environmental Engineering, Florida International University, 10555 W Flagler St., Suite 3680, Miami, FL 33174, USA
[c] Pacific Northwest National Laboratory, P.O. Box 999, K3-62, Richland, WA 99352, USA

ARTICLE INFO

*Article history:*
Received 28 November 2012
Received in revised form 22 May 2013
Accepted 23 May 2013
Available online 6 June 2013

Editor: J. Fein

*Keywords:*
Autunite
Dissolution
Uranium
Activation energy
Enthalpy
Bicarbonate

ABSTRACT

This research evaluated the effect of aqueous hydrogen carbonate solutions on the uranium rate of release from natural Ca-autunite and quantified the process kinetic rate law for a better prediction of the stability of autunite-group minerals. Testing was accomplished via a single-pass flow-through (SPFT) apparatus using buffered aqueous bicarbonate solutions (0.0005 to 0.003 M) at temperatures of 23–90 °C and pH values of 7–11. The release rate of uranium from Ca-autunite was directly correlated to increasing concentrations of hydrogen carbonate solutions and showed strong pH dependency. Ca-autunite kinetic rate law parameters were compared to the values obtained for synthetic Na-autunite. The power law coefficient and intrinsic rate constant were higher at pH 9–11 for Ca-autunite than for Na-autunite. The lower stability of Ca-autunite was attributed to the high Ca-autunite surface cracking, fractures and basal plane cleavages as compared to Na-autunite and the combined effect of the formation of aqueous uranyl–carbonate and calcium uranyl carbonate species as a driving force for uranium(VI) detachment and the formation of secondary Ca–P hydroxyapatite and uranyl phosphate mineral phases as a driving force for phosphate and calcium detachment controlling the net release of elements.

Published by Elsevier B.V.

## 1. Introduction

Globally, uranium (U) occurs as an essential component in different minerals and the majority of naturally occurring uranium deposits are oxides, silicates, vanadates, and phosphate minerals such as autunite (Burns, 1999). Uranium is one of the most frequently found radionuclides in groundwater as a result of reactor operations, nuclear fuel production and waste reprocessing (Riley et al., 1992). Autunite minerals $\{(X^m)_{2/m}[(UO_2)(PO_4)]_2 \bullet xH_2O\}$ are an important group known for their low solubility that largely controls the mobility of U in the subsurface. The autunite-group is very diverse, permits a wide range of cation and anion substitutions, and varying degrees of hydration (Burns, 1999). Many arid and semi-arid environments, including areas used for the storage of high-level radioactive waste at the U.S. Department of Energy (DOE) sites, contain elevated concentrations of sodium that in the presence of phosphorus (P) and uranium U(VI) rapidly form sodium uranyl phosphate phases. Injection of a soluble sodium tripolyphosphate amendment into the uranium contaminated groundwater and soil have been shown to effectively sequester uranium through the formation of insoluble Na uranyl phosphate solid phases. A sodium analog of autunite has been found in nature. Chernikov et al. (1957) conducted characterization of the hydrated sodium meta-autunite discovered in the Kuruk uranium deposit of northern Tajikistan and found that it is similar in properties to the autunite group. Mills et al. (2012) reported that metanatroautunite from the Lake Boga granite, Victoria, Australia, was similar to synthetic Na $[(UO_2)(PO_4)](H_2O)_3$ and featured identical corrugated polyhedral sheets as the meta-autunite-group minerals, consisting of corner-sharing uranyl square pyramids and phosphate tetrahedra.

Calcium, as one of most abundant metals in the earth's crust, promotes the formation of calcium-autunite, $Ca[(UO_2)(PO4)]_2 \bullet (H_2O)_{11}$. This phase has been recognized as the dominant form of autunite (Burns, 1999). The crystal structure contains the well-known autunite type sheet with composition $[(UO_2)(PO_4)]^-$, resulting from the sharing of equatorial vertices of the uranyl square bipyramids with the phosphate tetrahedra. The calcium atom in the interlayer is coordinated by seven $H_2O$ groups and two longer distances from uranyl ion oxygen atoms (Locock and Burns, 2003).

Fairchild (1929) showed that in artificial autunites sodium was replaced by calcium and the exchange reactions take place rapidly in Ca-rich environment with compounds of the autunite type. According to Anthony et al. (2000), two distinct changes occur during the exchange of sodium for calcium in the autunite structure. Primarily, two sodium cations are exchanged for the calcium ion to maintain the

* Corresponding author.
*E-mail address:* katsenov@fiu.edu (Y.P. Katsenovich).

0009-2541/$ – see front matter. Published by Elsevier B.V.
http://dx.doi.org/10.1016/j.chemgeo.2013.05.038

charge balance of the structure. The exchange of sodium for calcium is also associated with an increase in waters of hydration (Wellman et al., 2005). These changes in the chemical and structural composition of autunite raise questions on the impact of environmental factors on the stability of autunite-group minerals.

Literature data suggest the low solubility and high stability of many uranyl–phosphate minerals (Felmy et al., 2003; Gorman-Lewis et al., 2009). The solubility constant of the calcium form of autunite, log $K_{sp}$, has been measured as − 44.7 (Grenthe et al., 1992; Langmuir, 1997). A recent solubility study on natural Ca–U–P stability constant values for aqueous complexes yielded a log $K_{sp}$ value of − 48.36 with 2$\sigma$ uncertainty values of ± 0.03 (Gorman-Lewis et al., 2009). Associated species of reaction are shown in Eq. (1).

$$Ca(UO_2)_2(PO_4)_2 \cdot 3H_2O = 3H_2O + Ca^{2+} + 2PO_4^{3-} + 2UO_2^{2+} \quad (1)$$

Different environmental variables including temperature and pH have been extensively investigated (Wellman et al., 2006) on the dissolution of synthetic Na meta-autunite (herein designated as Na-autunite) and natural Ca meta-autunite minerals (herein designated as Ca-autunite). Their results indicated that meta-autunite dissolution kinetics is strongly dependent on pH and independent of temperature variation. Ca-rich carbonate-bearing subsurface environments, typical for the arid areas of the western U.S., afford the formation of aqueous calcium uranyl–carbonate and hydroxide complexes, which are mobile and promote U(VI) migration in natural waters (Clark et al., 1995; Kalmykov and Choppin, 2000; Bernhard et al., 2001). The strength of uranyl carbonate complexes makes the inorganic carbon species be the most effective extractant in terms of the dissolution rate and the extent of recovery of U from uranyl — bearing mineral phases (Perez et al., 2000; Sowder et al., 2001). Gudavalli, 2012, via single-pass flow-through (SPFT) experiments, investigated the rate of U(VI) release from Na-autunite, $Na[(UO_2)(PO_4)]\cdot 3H_2O$, as a function of bicarbonate solution concentrations ranging from 0.0005 M to 0.003 M in the pH range of 6–11 and temperature between 5 and 60 °C. The rate of U(VI) release from Na-autunite in the presence of low bicarbonate concentrations was increased over 300 fold when compared to the rate of U(VI) release in the absence of bicarbonate. Quantification of kinetic rate law parameters for the dissolution reaction of sodium meta-autunite suggested that activation energies were unaffected by temperature and bicarbonate solution concentrations but strongly depended on pH conditions (Gudavalli, 2012). Considering rapid exchange reactions of sodium for calcium in the autunite structure, the study of the effect of aqueous bicarbonate concentrations on the rate of U(VI) release from Ca-autunite can be extended to better understand U(VI) mobilization in groundwater.

The objectives of this research were to (i) investigate the effect of low concentrations of bicarbonate solutions on the dissolution of U(VI) from Ca-autunite via SPFT experiments and determine the U(VI) rate of release, (ii) quantify the kinetic rate law parameters of Ca-autunite dissolution, and (iii) compare the results with the dissolution of Na-autunite for better prediction of the bicarbonate impact on the release of U(VI) and the dissolution process of the autunite-group minerals. This information is critical for the prediction of autunite stability and long-term fate and transport of uranium in the subsurface.

## 2. Materials and methods

### 2.1. Autunite specimens

Synthesis of Na-autunite, $Na[(UO_2)(PO_4)]\cdot 3H_2O$, was followed by a modified direct precipitation method described by Wellman et al. (2005). Uranyl nitrate and sodium phosphate dibasic solutions were mixed in a volumetric ratio of 1:7.5 at 70 °C while stirring; heat was terminated after a yellowish green precipitate was formed. X-ray diffraction analysis was performed on the synthesized autunite mineral at 40 kV and 40 mA using a Bruker 5000D XRD instrument. Diffraction patterns were obtained using a copper radiation source with a tungsten filter. The sample was analyzed in the range of 2 to 35° for the 2-theta (2θ) with a 0.04° step increment and a two-second count time at each step. The XRD diffraction patterns were consistent with PDF# 049-0432 for Na-meta-autunite I (mAut I), $Na[(UO_2)(PO_4)]\cdot 3H_2O$, obtained from PNNL for comparison. The synthesized autunite solids were characterized by a JSM-5900-LV low vacuum scanning electron microscope (SEM) at 15 kV for identification of the particle sizes. The elemental composition and purity of the solids were determined via a Noran System Six Model 200 SEM energy dispersive X-ray spectroscopy (EDS). The Na:O:P:U atomic ratios of 1.08:5.69:1.00:1.04, determined by means of EDS analysis, corresponded to an ideal empirical formula of $Na[UO_2PO_4]$ as 1:6:1:1. Pre-experimental surface area analysis was conducted following the $N_2$-adsorbtion BET method (Brunauer et al., 1938) by using a Micromeritics ASAP 2020 surface and porosity analyzer at Pacific Northwest National Laboratory (PNNL). The structure of synthesized autunite solids, characterized by JSM-5900-LV low vacuum scanning electron microscope (SEM) at 15 kV, exhibited a smooth surface without distinctive cleavage planes (Fig. 1a).

Natural Ca-autunite, $Ca[(UO_2)(PO_4)]_2\cdot 3H_2O$, obtained from Excalibur Mineral Corporation (Peekskill, New York), was previously characterized using ICP-OES, ICP-MS analyses, X-ray diffraction and SEM/EDS to confirm the mineral composition, structure, and morphology as 98–99% pure autunite (Wellman et al., 2006). Scanning electron micrographs of Ca-autunite illustrate the multilayer structure resulting from the negatively charged $[(UO_2)(PO_4)]_2^{2-}$ layers. The morphology features perfect (001) basal, cleavage producing planes characteristic of autunite minerals (Anthony et al., 2000). As illustrated in the scanning electron micrographs displayed in Fig. 1b and c, surface cracking, fractures, and basal plane cleavage tended to be greater in Ca-autunite, resulting in a greater surface area compared to the Na-autunite counterpart. The autunite sample was powdered to have a size fraction of 75 to 150 μm or − 100 to + 200 mesh with an average surface area of 0.88 $m^2\ g^{-1}$.

### 2.2. Single-pass flow-through (SPFT) experiments

Mineral dissolution is a complex process consisting of a series of elementary reactions occurring at the mineral-water interface (Stamm and Wollast, 1990; Nagy, 1995; Sparks, 1999; Pablo et al., 1999). The release rate of elements from solids into solution is frequently controlled by kinetics. It has been accepted practice by geochemists to use the Transition State Theory (TST) that assumes that the dissolution rate is controlled by the desorption kinetics of an activated complex formed at the surface of solid phase (Lasaga, 1984). TST can be used to calculate the flux of elements released into the aqueous phase (Nagy, 1995). A general form of rate equation is based on the TST of chemical kinetics, centered on the prediction that the overall reaction rate is governed by the slowest elementary reaction, known as the rate-limiting step (Aagaard and Helgeson, 1982; McGrail et al., 1997). The reaction is given by

$$r = k\nu_i a_{H^+}^{\pm\eta} \exp\left(\frac{-E_a}{RT}\right)\left[1-\frac{Q}{K_g}\right]^{\sigma} \prod_j a_j^{n_i}, i = 1, 2, \ldots N \quad (2)$$

where $r$ is the dissolution rate in g $m^{-2}$ $d^{-1}$, $k$ is the intrinsic rate constant in g $m^{-2}$ $d^{-1}$, $\nu_i$ is the mass fraction of element $i$, $a_j$ is the activity of the $j$th aqueous species that acts as an inhibitor or catalyst, $E_a$ is the activation energy in kJ $mol^{-1}$, $R$ is the gas constant in kJ $mol^{-1}$ $K^{-1}$, $T$ is the temperature in K, $Q$ is the ion activity product, $K_g$ is the pseudo equilibrium constant, $\eta$ is the power law coefficient, and $\sigma$ is the Temkin coefficient.

The dependence of the dissolution rate of the Ca-autunite mineral on bicarbonate concentration was quantified via single-pass flow-through (SPFT) experiments conducted over a temperature range of 23° to 90 °C and a controlled pH range from 7 to 11. This test is designed to

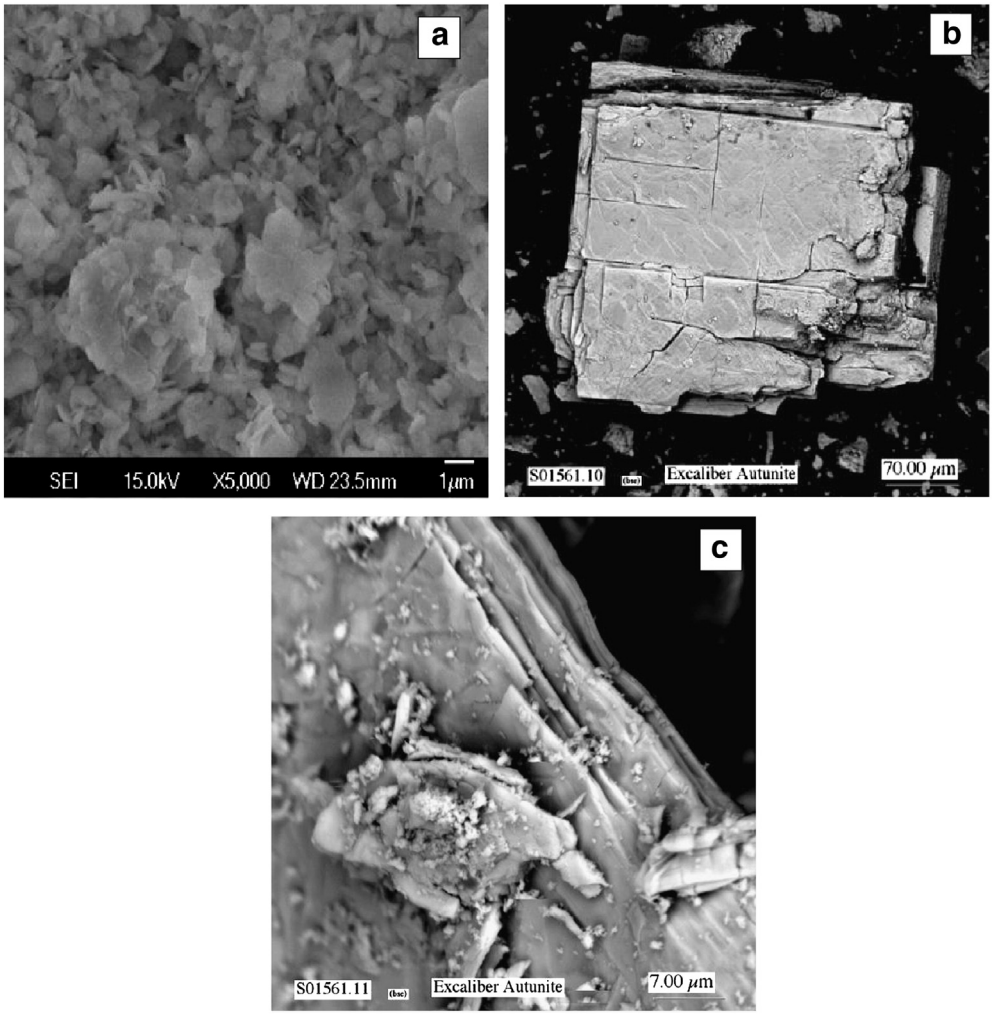


**Fig. 1.** (a) SEM images showing platy crystals of precipitated synthetic Na-autunite synthesized by the direct method. (b, c) SEM images of natural Ca-autunite obtained from Excalibur Mineral Corporation.

measure reaction rates under tightly controlled, dilute solution conditions by performing experiments at the forward rate, which is far from equilibrium conditions (McGrail et al., 1997). A schematic of the setup is shown in Fig. 2. A detailed description of the SPFT reactors are presented in McGrail et al., 1997; Pierce et al., 2005, 2008; Icenhower et al., 2006; and Wellman et al, 2006. A series of buffer compositions, all prepared with distilled, de-ionized water (DDIW), consisting of 0.01 M *tris (hydroxymethyl) aminomethane* (TRIS) buffered bicarbonate solutions with concentrations ranging from 0.0005 to 0.003 M, were used to investigate U(VI) release from natural Ca-autunite mineral over the pH (23 °C) interval of 7 to 11. 15.8 M concentrated trace-metal grade nitric acid ($HNO_3$) and 5 M lithium hydroxide (LiOH) solutions were used to adjust solutions to the target pH (Table S1). The 0.25 g of powdered autunite mineral resting at the bottom of the reactor interacted with the buffered bicarbonate solution. The effluent solution was continuously collected until steady state conditions were attained, which was accomplished after the transfer of approximately 8 reactor volumes. Collected aliquots samples were retained for pH measurements and concentration analysis of dissolved U(VI) via kinetic phosphorescence analyzer (KPA-11) (Chemcheck Instruments, Richland, WA).

The SPFT test was designed to limit the accumulation of reaction products using a sufficient ratio of the flow rate to the surface area of the mineral sample (q/S) to ensure the maximum dissolution rate or forward rate was achieved. The forward rate is then used to independently determine the effect of all other environmental variables on release rates. These conditions allow maintaining the chemical affinity term, $Q/K_g$, at a value near zero in Eq. (2). By observing changes in the dissolution rate over the range of experimental parameters tested, $k$, Ea, and $\eta$ can be easily obtained by means of standard non-linear regression.

### 2.3. Quantification of dissolution rate

The normalized dissolution rate of Ca-autunite solids was calculated from Eq. (3) when the system reached equilibrium (McGrail et al., 1997).

$$R_i = (C_i - C_{ib})\frac{q}{f_i S} \tag{3}$$

where: $R_i$ is the normalized dissolution rate for element $i$ (mol $m^{-2}$ $s^{-1}$), $q$ is flow rate, L $d^{-1}$, $C_i$ is concentration of component $i$ in the effluent (g $L^{-1}$), $C_{ib}$ is mean background concentration of component $i$ (g $L^{-1}$), $f_i$ is the mass fraction of the element in the metal (dimensionless), and S is the surface area of the sample ($m^2$).

The steady-state conditions were achieved after approximately eight reactor volumes exchanged and the concentrations of uranium released from natural Ca-autunite became invariant with respect to time for all pH and bicarbonate ranges tested.

The standard deviation of the dissolution rate was determined according to the uncertainty associated with each parameter shown

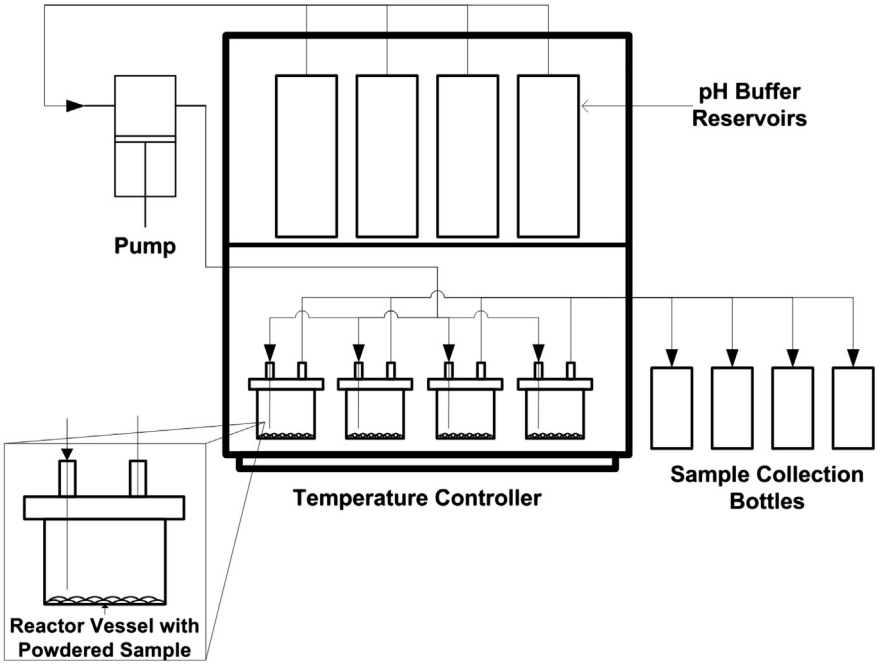


**Fig. 2.** Schematic of single-pass flow-through experimental setup.

in Eq. (3). Standard deviation for uncorrelated random errors is given by:

$$\sigma_f = \sqrt{\sum_{i=1}^{n} \left(\frac{\partial f}{\partial x_i}\right)^2 \sigma_i^2} \tag{4}$$

where: $\sigma_f$ — standard deviation of the function$f$; $x_i$ — parameter i; and $\sigma_i$ — standard deviation of parameter i.

Substituting Eq. (3) in Eq. (4) and converting to the relative standard deviation 2, $\widehat{\sigma}_r = {}^{\sigma_f}/_{x}$, yields

$$\sigma_r = \sqrt{\frac{(\widehat{\sigma}_c C_i^{out})^2 + (\widehat{\sigma}_b C_i^{in})}{(c_i^{out} + c_i^{in})^2} + \widehat{\sigma}_{fi}^2 + \widehat{\sigma}_s^2 + \widehat{\sigma}_q^2}. \tag{5}$$

Uncertainty associated with each parameter was considered when calculating the dissolution rate; relative errors included are final concentration (10%), background concentration (10%), mass distribution (5%), surface area (15%), and flow rate (5%). This error analysis results in typical $2\sigma$ uncertainties of approximately ±35% for SPFT-measured dissolution rates (or ±0.2 log units when reported as log10 rates) (Wellman et al., 2006). Actual flow rates, pH, temperature values, effluent uranium concentrations, surface areas and the rate of uranium releases are presented in Table S2. The experimental results were correlated by linear regression using SigmaPlot-11.2 (Systat Software Inc.).

### 2.4. Groundwater modeling

Steady state elemental concentrations in the effluent solution after the system reached equilibrium were used to identify the predominant uranium species in aqueous solution. The speciation modeling was performed by means of geochemical modeling software Visual MINTEQ v. 3.0 [maintained by J. Gustafsson at KTH, Sweden, available at http://www.lwr.kth.se/English/OurSoftware/vminteq/] using thermodynamic data from Grenthe et al (1992) and updated with the Nuclear Energy Agency's thermodynamic database for uranium (Guillaumont et al., 2003), calcium–uranyl–carbonate complexes (Dong and Brooks, 2006), and becquerelite dissolution data by Gorman-Lewis et al. (2008). The uranium speciation and solubility calculations are based on current knowledge and may have significant associated uncertainties.

## 3. Results and discussion

### 3.1. Effect of bicarbonate

The effect of bicarbonate on the dissolution of Ca-autunite was estimated from experimental results using:

$$r = k[\mathrm{HCO_3^-}]^{\eta} \tag{6}$$

$$\log r = \log k + \eta \log[\mathrm{HCO_3^-}] \tag{7}$$

where $r$ is the dissolution rate (mol $m^{-2}$ $s^{-1}$), $k$ is the intrinsic rate constant (mol $m^{-2}$ $s^{-1}$), $HCO_3^-$ is the concentration of pH-adjusted Tris-buffered bicarbonate solutions (mol $L^{-1}$) initially prepared for experiments, and $\eta$ is the power law coefficient (dimensionless). The concentration of the dissolved carbonate species needs to consider the change in speciation between $CO_2/HCO_3^-/CO_3^{2-}$ with pH in aqueous solution under experimental conditions. A non-linear regression was performed for each temperature with dissolution rates as a function of concentration of bicarbonate solutions to determine slope and the power law coefficient, $\eta$. The resulting regression coefficient over the entire data helped to define the intrinsic rate constant, $k$ (mol $m^{-2}$ $s^{-1}$).

Fig. 3 illustrates the rate of U(VI) release from Ca-autunite under the range of pH 7–11, across the aqueous bicarbonate concentrations tested and the temperature range of 23° to 90 °C. This figure depicts the strong effect of pH on the uranium rate of release, which is consistent with previous studies on the dissolution rate of autunite minerals (Wellman et al., 2006, 2007). At pH 7, the increase in the rate of U(VI) release was noted to be ~18 fold as the bicarbonate concentration increased from 0.3 mM to 3 mM. The value of the power law coefficient, $\eta$, calculated from the slope of U(VI) rate of release as 0.50 ± 0.12 was further used to estimate the intrinsic rate constant, $k$, of $1.09 \times 10^{-09}$ (mol $m^{-2}$ $s^{-1}$). Saturation indexes at pH 7 showed that potential secondary phases such as schoepite and β-$UO_2(OH)_2$

were under-saturated at all bicarbonate concentrations used in the experiments suggesting that the release of U(VI) is solely due to the dissolution of Ca-autunite. At pH 8 and 9, the rate of U(VI) release was observed to increase approximately 6.5 times with an increase in the concentration of bicarbonate solution by 17–65 fold, correspondingly, with respect to the rate of release at pH 7. The power law coefficients calculated from the slope of U(VI) release rate and the resulting intrinsic rate constant, $k$, at pH 8 and 9 are presented in comparison with similar parameters obtained for Na-autunite in Table 1. Calculations showed that at pH 9 values of $\eta$ and $k$ were 1.6 and 19 times higher for the Ca-autunite, compared to Na-autunite, respectively (Table 1). The rate of U(VI) release at pH 10 and 11 over the aqueous bicarbonate concentration interval tested was higher by approximately 18.5 fold and 14 fold, respectively, and by 300–400 fold with respect to the rate of U(VI) release at pH 7. For the same pH range, values of $\eta$ and $k$ were higher for the Ca-autunite by 1.8–2.8 and 126–484 times, correspondingly, compared to Na-autunite, indicative of the greater stability of Na-autunite. The values of the power law coefficient were observed to be invariant over the temperature interval, implying that the dissolution process within experimental error is independent of temperature (Fig. 3).

It was previously determined that the uranium release from Ca- and Na-autunite minerals is a surface-mediated reaction with the uranium

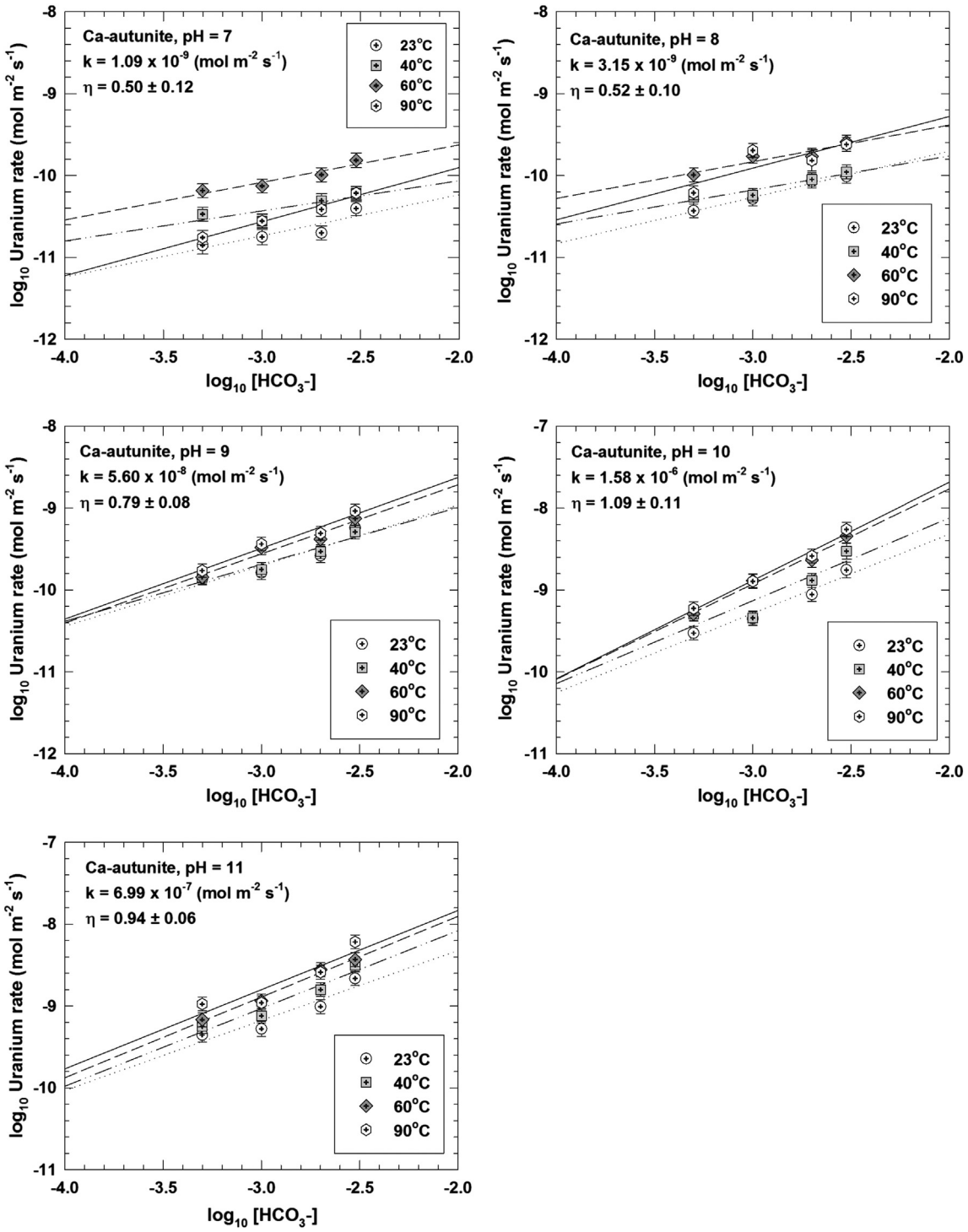


**Fig. 3.** Change in the rate of U(VI) release from Ca-autunite as a function of bicarbonate solution concentrations in the pH range of 6–11 and temperature between 23 °C and 90 °C.

polyhedrons (Wellman et al., 2006, 2007). This reaction mechanism schematically occurs in several steps with the fast attachment of the reactants to the mineral surface sites through fractures and cleavages of the mineral and then slow and rate-limiting detachment of metal species from the surface into solution (Stamm and Wollast, 1990; Nagy, 1995; Sparks, 1999). Uranyl ions release from Ca-autunite under the influence of bicarbonate ions proceeds by a two-step process: surface coordination of $HCO_3$ and $CO_3^{2-}$ on the U(VI) mineral surface and then detachment of the uranyl carbonate U(VI)-$CO_3^-$ and Ca-U(VI)-$CO_3^-$ species formed at the surface back in to solution (Pablo et al., 1999; Liu et al., 2004). The autunite minerals structure is characterized by the relatively weak forces holding successive sheets together. The liberation of U(VI) influences incongruent reactions to release Ca and P from the mineral structure and their presence in the aqueous solution is another possible driving force for Ca-autunite dissolution (Wellman et al., 2006). An increase in the aqueous bicarbonate concentrations at pH 8–9 correlated with a decrease in the saturation indices of potential secondary phases as schoepite and β-$UO_2(OH)_2$, suggesting a faster release of U(VI) from autunite under these conditions. Starting from pH 9, hydroxyapatite was super saturated at all bicarbonate concentrations; besides, the speciation modeling indicated that at pH 10 and 11, the system was potentially saturated with respect to various secondary Ca–P phases (Table 2). The other uranium oxyhydroxide phase, which could be potentially be formed due to the presence of Ca, is becquerelite $Ca(UO_2)_6O_4(OH)_6(H_2O)_8$. It was previously observed that schoepite has a tendency to incorporate cations into the interlayer spacings of the lattice and calcium is the most commonly incorporated cation in natural environments leading to the formation of becquerelite (Finch and Murakami, 1999). However, according to the speciation modeling, becquerelite remained under saturated at all tested conditions. At pH interval 7–11, highly soluble and stable uranyl–carbonate and calcium uranyl carbonate complexes, $UO_2(CO_3)_3^{4-}$ and $CaUO_2(CO_3)_3^{2-}$, became predominate aqueous species. The percentage of Ca–U–$CO_3$ species increased to about 10–27.7% in the pH range 9–11, while U–$CO_3$ species were ranging between 52 and 76%. Based on the information obtained from the Visual MINTEQ geochemical modeling software, the following elementary reactions are proposed for dissolution reactions at pH 7–10 (Eq. (8)) and pH 11 (Eq. (9)):

$$Ca_2[(UO_2)(PO_4)]_2xH_2O + HCO_3^- \rightarrow UO_2(CO_3)_3^{-4} + Ca(UO_2)(CO_3)_3^{-2} + HPO_4^{-2} + Ca^{+2} + xH_2O \quad (8)$$

$$Ca_2\left[(UO_2)\left(PO_4^{\ 4}\right)\right]_2 xH_2O + CO_3^- \rightarrow UO_2(CO_3)_3^{-4} + HPO_4^{-2} + CaPO_4^- + xH_2O. \quad (9)$$

The predominant uranyl species at all pHs tested was $UO_2(CO_3)_3^{-4}$, accounting for approximately 70% of the total uranyl species. $H_2PO_4^{-2}$ was the major phosphate species calculating for nearly 60% at all pH conditions tested. Calcium species distribution showed dependency on pH. At pH 7, the system was dominated by $Ca^{2+}$ ions while $CaUO_2(CO_3)_3^{-2}$ species became predominate at pH 8 to 10, representing approximately 95% and 80% of the total Ca species respectively. At pH 11, 85% of Ca was found in the form of $CaPO_4$.

In aqueous solution, the dissolved inorganic carbon is distributed among three species ($H_2CO_3$, $HCO_3$, and $CO_3$) as a function of pH. The distribution of carbonate species at known pH and pK's suggests that $HCO_3^-$ is the dominant carbonate species in the solution between pH 7.0–9.0 (Stumm and Morgan, 1996). As pH reaches 10–11, the fraction of $CO_3^{2-}$ in the dissolved carbonate species distribution increases. The percentages of [$HCO_3^-$] and [$CO_3^{2-}$] are calculated as 68% and 31.4% at pH 10 and 18% and 82% at pH 11, respectively. Therefore, the observed increase in the uranium rate of release with rising pH and concentration of buffered bicarbonate solutions could be explained by the increase of the $CO_3^{2-}$ species in aqueous solutions and the formation of strong and highly soluble U(VI)–carbonate and Ca–U(VI)–carbonate complexes.

As predicted by speciation modeling, the release of aqueous Ca and P-bearing species into solution during Ca-autunite dissolution was noted to increase as a function of pH. The concentration of Ca and P-bearing species increased 26 fold from $1.18 \times 10^{-05}$ mol $L^{-1}$ and $2.36 \times 10^{-05}$ mol $L^{-1}$ at pH 7 to $3.02 \times 10^{-04}$ mol $L^{-1}$ and $6.06 \times 10^{-04}$ mol $L^{-1}$ at pH 11, respectively. So, a combined effect of aqueous complex formation of uranyl–carbonate and calcium–uranyl–carbonate species as a driving force for uranyl detachment and the formation of secondary Ca–P hydroxyapatite and uranyl phosphate mineral phases as a driving force for phosphate and calcium detachment can control the net release of elements. Similar observations were noted in the bio-enhanced release of U(VI) from Ca-autunite in the presence of aqueous bicarbonate (Katsenovich et al., 2012).

Evaluation of the solid phase's surface morphology suggested that the synthetic Na-autunite did not exhibit cleavage planes prior to dissolution (Fig. 1). SEM images of reacted synthetic minerals have only revealed the minor formation of cleavage planes during the dissolution process, showing generally undisturbed post-experimental uranyl–phosphate sheets in the Na-autunite structure (Fig. 4a). Comparably, the crystals structure of post-reacted Ca-autunite showed a dramatic degree of distortion and layers separation (Fig. 4b,c). SEM evaluation of post-reacted synthetic and natural autunite presented no indication of secondary phase formation (Fig. 4a–c).

Perhaps surface structural differences between Na and Ca autunite minerals along with the potential formation of secondary uranyl phosphate phases and Ca–U–$CO_3$ aqueous species contribute to the increased rate of U(VI) dissolution observed via SPFT Ca-autunite dissolution experiments. The accessible gap (cleavage) between the Ca-autunite mineral sheet layers increases the probability that dissolution could occur through attack by aqueous bicarbonate and carbonate ions on the surface structural defects (Kalmykov and Choppin, 2000; Bernhard et al., 2001; Kerisit and Liu, 2010).

**Table 1**
Power law coefficients and intrinsic rate constants.

| pH | Ca-autunite | | Na-autunite[a] | |
|---|---|---|---|---|
| | $\eta$ | $k$ (mol $m^{-2}$ $s^{-1}$) | $\eta$ | $k$ (mol $m^{-2}$ $s^{-1}$) |
| 7 | 0.50 ± 0.12 | $1.09 \times 10^{-09}$ | 0.42 ± 0.13 | $3.62 \times 10^{-10}$ |
| 8 | 0.52 ± 0.10 | $3.15 \times 10^{-09}$ | 0.57 ± 0.04 | $1.48 \times 10^{-09}$ |
| 9 | 0.79 ± 0.08 | $5.60 \times 10^{-08}$ | 0.48 ± 0.12 | $2.86 \times 10^{-09}$ |
| 10 | 1.09 ± 0.11 | $1.58 \times 10^{-06}$ | 0.39 ± 0.03 | $3.26 \times 10^{-09}$ |
| 11 | 0.94 ± 0.06 | $6.99 \times 10^{-07}$ | 0.51 ± 0.02 | $5.51 \times 10^{-09}$ |

[a] Gudavalli (2012).

### 3.2. Estimation of thermodynamic parameters (activation energy of dissolution)

An important factor affecting the dissolution rate is activation energy, $E_a$, which depends on the nature of chemical reactions. Fast reactions have small activation energy and those with large activation energy usually progress slowly. Previous studies showed that pH has a pronounced effect on activation energy (Zhang et al., 2001). Bemer (1978) and Jordan and Rammensee (1996) reported that the activation energy can help identify the rate-controlling process of dissolution: activation energy values lower than 20 kJ $mol^{-1}$ represent surface diffusion as the rate-controlling process. Surface controlled dissolution usually results in higher activation energy; Lasaga (1984) reported that the surface controlled dissolution of silicates have activation energies in the range of 60–80 kJ $mol^{-1}$, and similar activation energy values (72–86 kJ $mol^{-1}$) were reported by various authors for alkaline earth fluorides whose dissolution rates are believed to be surface controlled. Previous studies on uranium-bearing materials suggested a

**Table 2**
Saturation indices of mineral phases as a function of pH and concentration of bicarbonate solutions.

| pH | $HCO_3^-$ (M) | Schoepite | β-$UO_2(OH)_2$ | Hydroxyapatite | β-$Ca_3(PO_4)_2$ | $Ca_3(PO_4)_2$ (am2) | $Ca_3(PO_4)_2$ (am1) | $Ca_4H(PO_4)_3 \cdot 3H_2O$(s) | $(UO_2)_3(PO_4)_2$(s) |
|---|---|---|---|---|---|---|---|---|---|
| 7 | 0.0005 | 0.057 | −0.173 | | | | | | 2.904 |
| | 0.001 | −0.179 | −0.409 | | | | | | 2.275 |
| | 0.002 | −0.528 | −0.757 | | | | | | 1.856 |
| | 0.003 | −0.758 | −0.988 | | | | | | 1.587 |
| 8 | 0.0005 | 0.335 | 0.106 | −0.942 | | | | | 0.98 |
| | 0.001 | 0.011 | −0.219 | 0.575 | | | | | 0.5 |
| | 0.002 | −0.471 | −0.7 | 2.898 | | | | | −0.232 |
| | 0.003 | −0.741 | −0.971 | 3.275 | | | | | −0.378 |
| 9 | 0.0005 | 0.586 | 0.356 | 6.386 | −0.69 | −1.526 | −4.285 | −3.248 | −1.078 |
| | 0.001 | 0.361 | 0.132 | 6.915 | −0.323 | −1.16 | −3.918 | −2.678 | −1.261 |
| | 0.002 | 0.034 | −0.196 | 8.487 | 0.669 | −0.168 | −2.926 | −1.275 | −1.757 |
| | 0.003 | −0.584 | −0.814 | 8.716 | 0.845 | 0.008 | −2.75 | −0.975 | −3.227 |
| 10 | 0.0005 | 0.652 | 0.422 | 14.551 | 3.928 | 3.091 | 0.333 | 2.44 | −3.695 |
| | 0.001 | 0.607 | 0.377 | 13.598 | 3.376 | 2.539 | −0.219 | 1.737 | −3.63 |
| | 0.002 | 0.344 | 0.114 | 12.11 | 2.512 | 1.675 | −1.083 | 0.632 | −4.136 |
| | 0.003 | −0.991 | −1.221 | 11.935 | 2.393 | 1.557 | −1.202 | 0.453 | −8.272 |
| 11 | 0.0005 | 0.265 | 0.035 | 15.229 | 3.923 | 3.087 | 0.328 | 1.749 | −8.966 |
| | 0.001 | 0.215 | −0.015 | 14.877 | 3.717 | 2.88 | 0.122 | 1.482 | −9.068 |
| | 0.002 | 0.055 | −0.175 | 14.381 | 3.431 | 2.594 | −0.164 | 1.118 | −9.437 |
| | 0.003 | −0.333 | −0.563 | 14.155 | 3.284 | 2.447 | −0.311 | 0.903 | −10.717 |

surface controlled dissolution mechanism for measured activation energies calculated in the range of 12–60 kJ $mol^{-1}$ (Scott et al., 1977; Pablo et al., 1999; Zhang et al., 2001). In this study, the effect of bicarbonate and carbonate ions on the activation energy of the dissolution reactions of Ca-autunite in a wide range of pH and temperatures is conducted by comparison with $E_a$ values for Na-autunite dissolution reported by Gudavalli (2012).

Activation energy values were estimated using a modified transition state theory equation describing the rate of reaction as a function of temperature, and the activities of the rate enhancing or inhibiting species, described as:

$$r = ke^{\frac{-E_a}{RT}}[HCO_3^-]^{\eta} \quad (10)$$

where $r$ is the dissolution rate (mol $m^{-2}$ $s^{-1}$) experimentally determined from SPTF tests, $k$ is the intrinsic rate constant (mol $m^{-2}$ $s^{-1}$), $[HCO_3^-]$ is the concentration of bicarbonate solutions (mol $L^{-1}$), $\eta$ is the power law coefficient (dimensionless), $E_a$ is activation energy (J $mol^{-1}$), $R$ is the universal gas constant (J $mol^{-1}$ $K^{-1}$), and $T$ is temperature (K). Calculations were conducted for each tested pH value.

At constant concentrations of bicarbonate solution, the normal logarithmic values of the rate of dissolution (ln $r$) were plotted against the values of inverse temperature ($T^{-1}$) as shown in Fig. 5. The reaction rate constant at a slope close to zero was most pronounced at pH 9, indicating no rate dependency on the temperature. A negative slope found at pH 7 shows an increasing reaction rate with increasing temperature. At pH 7 and 8, curves of different bicarbonate solution concentrations plotted close together, indicative of a weak effect of solution $HCO_3^-$ concentrations on the U(VI) rate of release. Whereas, at pH 10 and 11, curves separated from each other on the plot a sign that the rate of U(VI) release is much more rapid when $CO_3^{2-}$ became the predominate inorganic carbon species in the aqueous solution. The slope of the linear regression line at each pH value was calculated and the data is presented in Table 3. Data comparison for Ca-autunite with estimates obtained for Na-autunite revealed a weak dependency of the dissolution rate on the temperature for both materials. The average activation energy at pH 7 for Ca-autunite was estimated to be 25.50 kJ $mol^{-1}$. This suggests that the rate-limiting step of the reaction during the dissolution process is probably controlled by the surface bond-breakage of U–$CO_3$ and Ca–U–$CO_3$ ions occurring at the solid/liquid interface by which surface bound ions move into solution. This measure is also in agreement with the average activation energy value reported for Na-autunite at pH 7 (26.86 kJ $mol^{-1}$). The average values of activation energy for Ca-autunite at pH 8–11 were estimated in the range of 8–18 kJ $mol^{-1}$; the low requirements of energy to initiate the dissolution reaction are indicative of an increasing rate of U(VI) release in these conditions. The dissolution is faster at higher pH; so, activated energies in this range are suggestive of mass transfer as the rate-limiting step of the reaction leading to the crystal sheets cracking or splitting apart (Brantley et al., 2008). These values are similar to those reported for Na-autunite, and the calculated activation energies

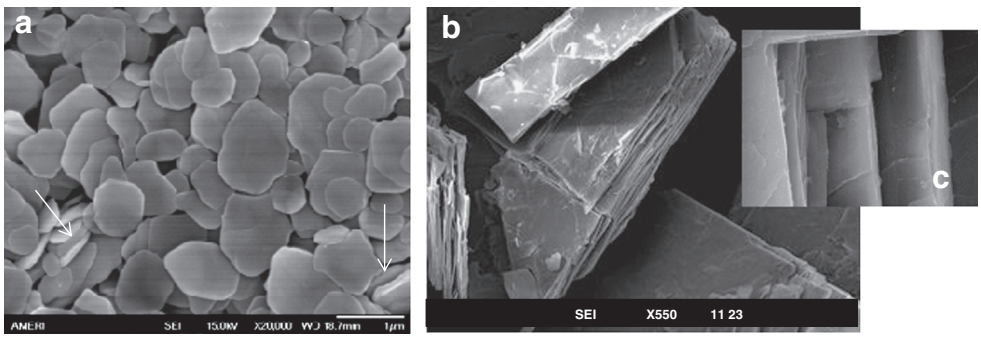


**Fig. 4.** Image of post-reacted autunite minerals. (a) Na-autunite at 20,000× showing minor formation of cleavage planes (white arrows) during the dissolution process. (b) Post-reacted Ca-autunite showing a dramatic degree of distortion and layers separation (×550). (c) Post-reacted Ca-autunite showing layers separation (×10,000).

for both Ca and Na autunite are in good agreement with those reported in the literature for similar materials (Zhang et al., 2001; Heisbourg et al., 2003).

The pseudo equilibrium constant, $K_g$, was estimated using Eq. (9), based on the assumption that the concentration of bicarbonate is the rate limiting factor that controls the reaction; where $r$ is the rate of dissolution (g $m^{-2}$ $d^{-1}$) and [$HCO_3^-$] is the concentration of bicarbonate solutions (M).

$$r = K_g\left[HCO_3^-\right] \tag{11}$$

The values of U(VI) rate of release (Y-axis) at different pH values were plotted against variations of concentration of bicarbonate solutions (X-axis) as shown in Fig. 6. The resulting slopes of the regression lines provided values of $K_g$ and are listed in Table 4.

Enthalpy is a unique characteristic measured for each material of a specific composition. Enthalpy of the system was evaluated using the correlation between the pseudo equilibrium constant, enthalpy, and the temperature of the system, described as:

$$\Delta H = -RT\ln K_g \tag{12}$$

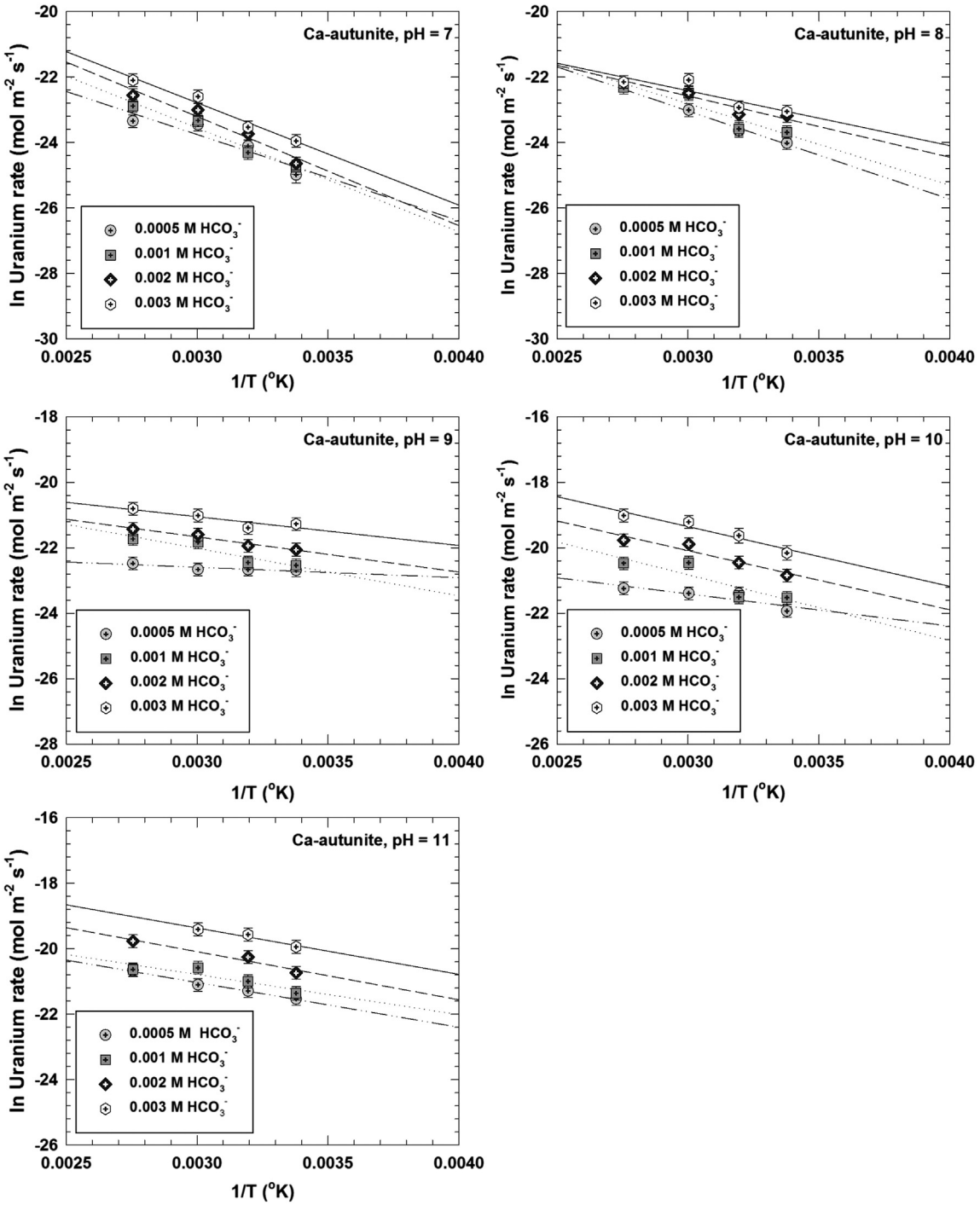


**Fig. 5.** ln of uranium release rate from Ca-autunite in the pH range 6–11 and concentrations of bicarbonate solutions ranging from 0.0005 M to 0.003 M versus values of inverse temperature. Activation energies were calculated as the slope of the linear regression line at each pH value.

**Table 3**
Changes in activation energies of autunite dissolution.

| $[HCO_3^-]$(M) | Ca-autunite | | | | Na-autunite[a] | | | |
|---|---|---|---|---|---|---|---|---|
| | 0.0005 | 0.001 | 0.002 | 0.003 | 0.0005 | 0.001 | 0.002 | 0.003 |
| pH | $E_a$ (kJ mol$^{-1}$) | | | | $E_a$ (kJ mol$^{-1}$) | | | |
| 7 | 21.87 | 26.39 | 27.72 | 26.00 | 28.285 | 30.426 | 24.872 | 23.882 |
| 8 | 22.41 | 20.72 | 15.57 | 13.95 | 9.824 | 16.872 | 18.751 | 17.091 |
| 9 | 2.63 | 13.07 | 8.95 | 7.32 | 11.417 | 16.553 | 14.983 | 13.863 |
| 10 | 8.17 | 16.68 | 15.05 | 15.17 | 4.031 | 9.028 | 7.627 | 7.579 |
| 11 | 11.39 | 10.19 | 12.23 | 11.78 | 14.831 | 12.947 | 12.955 | 11.511 |

[a] Gudavalli (2012).

**Table 4**
Pseudo equilibrium constants and enthalpy values at various pH.

| pH | Ca-autunite | | Na-autunite[a] | |
|---|---|---|---|---|
| | $K_g$ | ΔH (kJ mol$^{-1}$) | $K_g$ | ΔH (kJ mol$^{-1}$) |
| 7 | 0.65 | 28.58 | 0.16 | 19.39 |
| 8 | 0.79 | 11.83 | 0.35 | 17.24 |
| 9 | 4.20 | 11.90 | 1.39 | 24.80 |
| 10 | 25.97 | 15.88 | 1.34 | 12.44 |
| 11 | 27.75 | 13.84 | 1.30 | 9.41 |

[a] Gudavalli (2012).

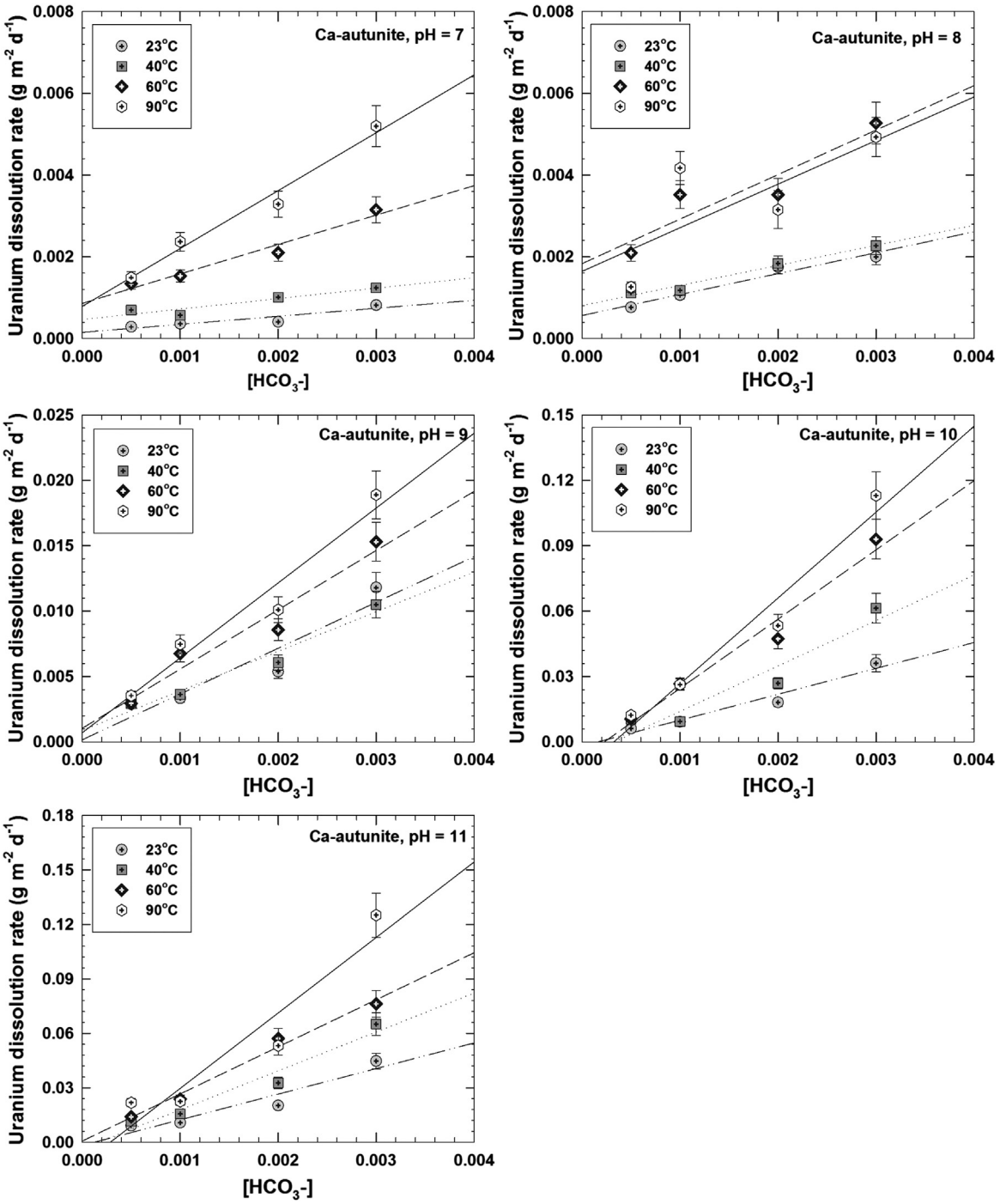


**Fig. 6.** Uranium release rate as a function of bicarbonate solution concentrations at various pH values. The resulting slopes of the regression lines provided values of $K_g$. Please note different scaling of the y-axes.

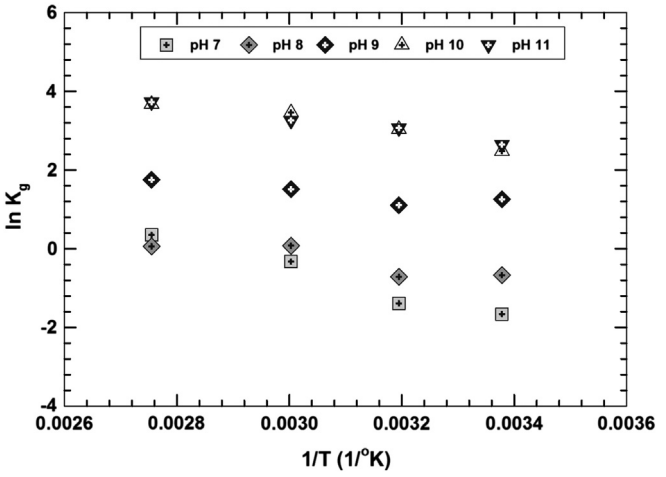


**Fig. 7.** Changes in the pseudo equilibrium constant as a function of inverse temperature. A slope of a linear graph with inverse temperature ($T^{-1}$) on the X-axis and the normal logarithmic values of pseudo equilibrium constant, ln $K_g$, on the Y-axis were used to estimate the enthalpy of the system at various pH values.

where ΔH is the enthalpy (J $mol^{-1}$), $R$ is the universal gas constant (J $mol^{-1}$ $K^{-1}$), and $T$ is temperature (°K). A slope of a linear graph with inverse temperature ($T^{-1}$) on the X-axis and the normal logarithmic values of pseudo equilibrium constant, ln $K_g$, on the Y-axis (Fig. 7) were used to estimate the enthalpy of the system at various pH values (Table 4).

The pseudo equilibrium rate constant values pertaining to Ca-autunite were found to be 4 times higher at low pH values (7–9) and 21 times higher at high pH values (10–11) than that for Na-autunite (Table 4). This data suggests that the reaction occurred slowly at low pH values and significantly faster at high pH values. A similar trend was shown by the intrinsic rate constant values. The change in enthalpy of Ca-autunite was found to be 0.5–1.5 times higher compared to the value of Na-autunite (Table 4). This change might not be significant enough to justify any principal differences in the uranium release reaction mechanisms; however, it correlates with the trend shown by the intrinsic rate constant pertaining to Ca-autunite dissolution suggesting higher U release from this phase. Geochemical modeling indicated, that Ca-autunite dissolution results in lager number of secondary phases that may form compared to Na-autunite. Perhaps, the liberation of phosphorus and the potential formation of calcium–phosphate secondary phases contribute to a higher enthalpy change associated with the dissolution of Ca-autunite.

The theoretical rate of uranium release was calculated, taking into account experimentally determined parameters associated with Eq. (2), including estimated activation energies and $K_g$ values. The theoretically determined rate of U(VI) release differs from the experimentally determined values within an error range ±10%.

## 4. Conclusions

The rate of dissolution of Ca-autunite was evaluated under bicarbonate concentrations ranging from 0.0005 to 0.003 M, pH 7 to 11 and temperature variations from 23 to 90 °C via single-pass flow-through cell experiments. The power law coefficient ($\eta$) for Ca-autunite in the range of the experimental parameters tested was observed between 0.5 and 1.0. Similar to Na-autunite, there was no quantifiable dependency of Ca-autunite dissolution on temperature. The rate of U(VI) release was observed to be the slowest reaction of the autunite dissolution. The activation energy ($E_a$) data at pH 7 suggests that the rate of dissolution is probably controlled by the surface chemical reactions occurring at the solid/liquid interface while, at pH 8–11, the low requirements of energy to initiate a dissolution reaction are indicative of a faster rate of U(VI) release due to cracking and splitting of the crystal sheets, achieved by mass transfer reactions. Pseudo equilibrium and enthalpy data showed that the dissolution process is slower at pH 7–8 and at higher pH the speed of dissolution increased. The kinetic rate law parameters for Ca-autunite were found to be higher than that for Na-autunite, suggesting a higher stability of Na-autunite. These differences were due to the active surface features of Ca-autunite and the formation of aqueous calcium uranium carbonate species, and the potential occurrence of mineral phases as secondary Ca–P hydroxyapatite and uranyl phosphate altering the solution saturation state. The dissolution rate data indicates that low concentrations of bicarbonate in the subsurface environments can impact the stability of the uranyl phosphate minerals. The information presented here provides critical fundamental aspects to refine the bulk kinetic parameters currently being used to predict autunite minerals stability and the fate of uranium in the subsurface.

## Acknowledgments

Funding for this work was provided by the U.S. Department of Energy Office of Environmental Management under grant DE-EM0000598. This manuscript was prepared in collaboration with the Deep Vadose Zone — Applied Field Research Initiative at the Pacific Northwest National Laboratory. The Pacific Northwest National Laboratory is operated by Battelle Memorial Institute for the Department of Energy (DOE) under Contract DE-AC05-76RL01830. We gratefully acknowledge the efforts of K. Parker from Pacific Northwest National Laboratory for his help with the surface area analysis of synthetic autunite; and A. Henao for his assistance in conducting KPA and ICP-OES analysis. The authors also acknowledge Dr. Y. Liu from the FIU Advanced Materials Engineering Research Institute (AMERI) and R. Lapierre and T. Beasley from FCAEM for their assistance with the SEM/EDS analysis.

We are grateful to two anonymous reviewers for their insightful and valuable comments on an earlier version of this manuscript.

## Appendix A. Supplementary data

Supplementary data to this article can be found online at http://dx.doi.org/10.1016/j.chemgeo.2013.05.038.

## References

Aagaard, P., Helgeson, H.C., 1982. Thermodynamic and kinetic constraints on reaction rates among minerals and aqueous solutions. I. Theoretical considerations. American Journal of Science 282, 237–285.
Anthony, J.W., Bideaux, R.A., Bladh, K.W., Nichols, M.C., 2000. Arsenates, Phosphates, Vanadates. Mineral Data Publishing 680.
Bemer, R.A., 1978. Rate control of mineral dissolution under earth surface conditions. American Journal of Science 278, 1235–1252.
Bernhard, G., Geipel, G., Reich, T., Brendler, V., Amayri, S., Nitsche, H., 2001. Uranyl(VI) carbonate complex formation: validation of the $Ca_2UO_2(CO_3)_3$ (aq) species. Radiochimica Acta 89, 511.
Brantley, S.L., Kubicki, J.D., White, A.F., 2008. Kinetics of Water–Rock Interactions. Springer Science Business Media, LLC 825.
Brunauer, S., Emmett, P.H., Teller, E., 1938. Adsorption of gases in multimolecular layers. Journal of the American Chemical Society 60, 309–319.
Burns, P.C., 1999. The crystal chemistry of uranium. Reviews in Mineralogy and Geochemistry 38, 23–90.
Chernikov, A.A., Krutetskaya, O.V., Organova, N.I., 1957. Natroautunite. Atomic Energy 3 (2), 901–905. http://dx.doi.org/10.1007/BF01480073.
Clark, D.L., Hobart, D.E., Neu, M.P., 1995. Actinide carbonate complexes and their importance in actinide environmental chemistry. Chemical Reviews 95, 25.
Dong, W., Brooks, S.C., 2006. Determination of the formation constants of ternary complexes of uranyl and carbonate with alkaline earth metals ($Mg^{2+}$, $Ca^{2+}$, $Sr^{2+}$, and $Ba^{2+}$) using anion exchange method. Environmental Science & Technology 40 (15), 4689–4695. http://dx.doi.org/10.1021/es0606327.
Fairchild, J.G., 1929. Base exchange in artificial autunites. American Mineralogist 4, 265–275.
Felmy, A.R., Xia, Y., Wang, Z., 2003. The solubility product of $NaUO_2PO_4 * H_2O$ determined on phosphate and carbonate solutions. Radiochimica Acta 93, 401–408.
Finch, R., Murakami, T., 1999. Systematic and paragenesis of uranium minerals (in uranium: mineralogy, geochemistry and the environment). Reviews in Mineralogy 38, 91–179.
Gorman-Lewis, D., Fein, J.B., Burns, P.C., Szymanowski, J.S., Converse, J., 2008. Solubility measurements of the uranyl oxide hydrate phases metaschoepite, compreignacite,

Na–compreignacite, becquerelite, and clarkeite. The Journal of Chemical Thermodynamics 40, 980–990.
Gorman-Lewis, D., Shvareva, T., Kubatko, K., Burns, P., Wellman, D.M., Amara, B., Szymanowski, J.S., Navrotsky, A., Fein, J.B., 2009. Thermodynamic properties of autunite, uranyl hydrogen phosphate, and uranyl orthophosphate from solubility and calorimetric measurements. Environmental Science and Technology 43, 7416–7422.
Grenthe, I., Fuger, J., Konings, R.J.M., Lemire, R.J., Muller, A.J., Nguyen-Trung, C., Wanner, H., 1992. Chemical Thermodynamics of Uranium. Elsevier, Amsterdam.
Gudavalli, R., 2012. Effect of pH and temperature on the carbonate promoted dissolution of sodium meta-autunite. Florida International University Miami, FL (Ph.D. dissertation).
Guillaumont, R., Fanghänel, T., Fuger, J., Grenthe, I., Neck, V., Palmer, D.A., Rand, M.H., 2003. Chemical Thermodynamics, OECD Nuclear Energy Agency, 5. Elsevier (919 pp).
Heisbourg, G., Hubert, S., Dacheux, N., Ritt, J., 2003. The kinetics of dissolution of $Th_{1-x}U_xO_2$ solid solutions in nitric media. Journal of Nuclear Materials 321 (2–3), 141–151.
Icenhower, J.P., Strachan, D.M., McGrail, B.P., Scheele, R.D., Rodriguez, E.A., Steele, J.L., Legore, V.L., 2006. Dissolution kinetics of pyrochlore ceramics for the disposition of plutonium. American Mineralogist 91 (1), 39–53.
Jordan, G., Rammensee, W., 1996. Dissolution rates and activation energy for dissolution of brucite (001): a new method based on the microtopography of crystal surfaces. Geochimica et Cosmochimica Acta 60 (24), 5055–5062.
Kalmykov, S.N., Choppin, G.R., 2000. Mixed $Ca^{2+}/UO_2^{2+}/CO_3^{2-}$ complex formation at different ionic strengths. Radiochim. Acta 88, 603.
Katsenovich, Y.P., Carvajal, D.A., Wellman, D.M., Lagos, E.L., 2012. Enhanced U(VI) release from autunite mineral by aerobic Arthrobacter sp. in the presence of aqueous bicarbonate. Chemical Geology 308–309, 1–9.
Kerisit, S., Liu, C., 2010. Molecular simulation of the diffusion of uranyl carbonate species in aqueous solution. Geochimica et Cosmochimica Acta 74 (17), 4937–4952.
Langmuir, D., 1997. Aqueous Environmental Geochemistry. Prentice-Hall, Inc.
Lasaga, A.C., 1984. Chemical kinetics of water–rock interactions. Journal of Geophysical Research B6, 4009–4025.
Liu, C., Zachara, J.M., Qafoku, O., Mckinley, J.P., Heald, S.M., Wang, Z., 2004. Dissolution of uranyl microprecipitates in subsurface sediments at Hanford Site, USA. Geochimica et Cosmochimica Acta 68 (22), 4519–4537.
Locock, A.J., Burns, P.C., 2003. The crystal structure of synthetic autunite, $Ca[(UO_2)(PO_4)]_2(H_2O)_{11}$. American Mineralogist 88, 240–244.
McGrail, B.P., Ebert, W.L., Bakel, A.J., Peeler, D.K., 1997. Measurement of kinetic rate law parameters on a Na–Ca–Al borosilicate glass for low-activity waste. Journal of Nuclear Materials 249 (2), 175–189.
Mills, S.J., Kamp, A.R., Birch, W.D., 2012. The crystal structure of metanatroautunite, $Na[(UO_2)(PO_4)](H_2O)_3$, from the Lake Boga Granite, Victoria, Australia. American Mineralogist 97, 735–738.
Nagy, K.L., 1995. Dissolution and precipitation kinetics of sheet silicates. In: White, A.F., Brantley, S.L. (Eds.), Chemical Weathering Rates of Silicate Minerals. Mineralogical Society of America, Washington, D. C., pp. 173–233.
Pablo, J.D., Casas, I., Gimenez, J., Molera, M., Rovira, M., Duro, L., 1999. The oxidative dissolution mechanism of uranium dioxide. I. The effect of temperature in hydrogen carbonate medium. Geochemistry. Cosmochiica Acta 63, 3097–3103.
Perez, I., Casas, I., Martin, M., Bruno, J., 2000. The thermodynamics and kinetics of uranophane dissolution in bicarbonate test solutions. Geochemistry. Cosmochiica Acta 64, 603–608.
Pierce, E.M., Icenhower, J.P., Serne, R.J., Catalano, J.G., 2005. Experimental determination of $UO_2$(cr) dissolution kinetics: effects of solution saturation state and pH. Journal of Nuclear Materials 345, 206–218.
Pierce, E.M., Rodriguez, E.A., Calligan, L.J., Shaw, W.J., McGrail, B.P., 2008. An experimental study of the dissolution rates of simulated aluminoborosilicate waste glasses as a function of pH and temperature under dilute conditions. Applied Geochemistry 23, 2559–2573.
Riley, R.G., Zachara, J.M., Wobber, F.J., 1992. Chemical Contaminants on DOE Lands and Selection of Contaminant Mixtures for Subsurface Science Research. U.S. Department of Energy, Office of Energy Research, Washington. DC.
Scott, P.D., Glasser, D., Nico, M.J., 1977. Kinetics of dissolution of β-uranium trioxide in acid and carbonate solutions. J. Chem. Soc. Dalton Trans. 20, 1939–1946.
Sowder, A.G., Clark, S.B., Fjeld, R.A., 2001. The impact of mineralogy in the U(VI)-Ca-$PO_4$ system on the environmental availability of uranium. Journal of Radioanalytical and Nuclear Chemistry 248 (3), 517–524.
Sparks, D.L., 1999. Kinetics and mechanisms of chemical reactions at the soil mineral/water interface, Soil Physical Chemistry, 2nd ed. CRC Press LLC.
Stamm, W., Wollast, R., 1990. Coordination chemistry of weathering. Kinetics of the surface — control dissolution of oxide minerals. Reviews of Geophysics 28, 53–60.
Stumm, W., Morgan, J., 1996. Aquatic Chemistry: Chemical Equilibria and Rates in Natural Waters, 3rd ed. John Wiley & Sons, Inc., New York (1022p).
Wellman, D.M., Catalano, J.G., Icenhower, J.P., Gamerdinger, A.P., 2005. Synthesis and characterization of sodium meta-autunite, $Na[UO_2PO_4] \cdot 3H_2O$. Radiochimica Acta 93, 393–399.
Wellman, D.M., Icenhower, J.P., Gamerdinger, A.P., Forrester, S.W., 2006. Effects of pH, temperature and aqueous organic material on the dissolution kinetics of meta-autunite minerals, $(Na, Ca)_{2-1}[(UO_2)(PO_4)]_2 \cdot 3H_2O$. American Mineralogist 91, 143.
Wellman, D.M., Gunderson, K.M., Icenhower, J.P., Forrester, S.W., 2007. Dissolution kinetics of synthetic and natural meta-autunite minerals, $X_{3-n}^{(n)+}[(UO_2)(PO_4)]_2 \cdot xH_2O$, under acidic conditions. Geochemistry, Geophysics, Geosystems 8, 16.
Zhang, Y., Hart, K.P., Bourcier, W.L., Day, R.A., Colella, M., Thomas, B., Aly, Z., Jostsons, A., 2001. Kinetics of uranium release from Synroc phases. Journal of Nuclear Materials 289 (3), 254–262.